A Two-Microphone Method for the Determination of the Mode Amplitude Distribution in High-Frequency Ducted Broadband Sound Fields

P. F Joseph

Institute of Sound and Vibration Research. University of Southampton, Southampton SO17 1BJ, UK.

This paper describes a measurement technique that allows the modal amplitude distribution to be determined in ducts with mean flow and reflections. The method is based only on measurements of the acoustic pressure two-point coherence at the duct wall. The technique is primarily applicable to broadband sound fields in the high frequency limit and whose mode amplitudes are mutually incoherent. The central assumption underlying the technique is that the relative mode amplitude distribution is independent of frequency. The two-microphone method proposed in this paper is also used to determine the transmitted sound power and far field pressure directivity.

Nomenclature

a	=	Duct radius
$\overline{a_\pm^2}$	=	normalized mean square mode amplitude distribution for positive and negative propagating modes
c	=	Speed of sound
k	=	ω/c
k_{mn}	=	axial wavenumber of mode mn
n	=	modal density function (Eq. 11)
r	=	radial coordinate
p	=	acoustic pressure
x	=	axial coordinate
$\mathbf{y}$	=	Position on the duct cross section
$\mathbf{y}_a$	=	Position on the duct wall
A	=	Duct area
A_{mn}	=	pressure amplitude of mode mn
F	=	Sound power factor (Eq. 32, 33)
M	=	Mach number
N	=	number of modes with 'α' values of between -1 and α
N	=	mode amplitude distribution normalisation factor
N	=	Total number of propagating modes at particular frequency
R	=	far field radial position from centre of the duct
$R(\alpha)$	=	Reflection coefficient
S_{11}	=	Pressure Power Spectral Density at duct wall
S_{12}	=	Pressure Cross Spectral Density at duct wall

45	$S_{ff}(\omega,\theta)$	=	Pressure PSD of far field radiation
46	$S(\omega)$	=	*source term (Eq. 7)*
47	$W(\omega)$	=	total transmitted sound power spectrum
48	$W^{\pm}(\omega)$	=	Upstream and downstream transmitted power
49	α	=	cuton ratio (Eq. 3)
50	β	=	Lorentz factor
51	δ	=	reflection factor
52	κ_{mn}	=	transverse modal wavenumber
53	θ	=	circumferential coordinate
54	ρ	=	mass density of air
55	ω	=	angular frequency
56	$\hat{\omega}$	=	non-dimensional frequency (Eq. 16)
57	ω_{mn}	=	natural frequency of mode *mn*
58	θ	=	polar coordinate of far field observer
59	Γ_{mn}	=	Mode normalization factors
60	$\Omega^{\pm}$	=	Sound power factors (Eq. (29, 30))
61	Ψ_{mn}	=	ortho-normal mode shape function
62	ψ_{12}	=	complex coherence function (Eq. 22)

63
64
65
66   ## I. INTRODUCTION

67

68   This paper deals with a measurement technique that allows the distribution of mode amplitudes to be

69   determined as a function of their cuton ratio in a hard walled duct containing an axial uniform mean flow.

70   Measurement of this mode distribution function then allows for estimation of the sound power transmitted

71   along the duct and of the directivity of the far field pressure radiated from the end of the duct. The unique

72   feature of this method is that it requires only measurements of the coherence function between two closely

73   spaced acoustic pressure measurements made at the duct wall and is applicable in the high frequency limit

74   where conventional mode detection methods fail since they require an unrealistically large numbers of

75   microphones. A preliminary version of this method was presented by the author in Joseph[1].

76

77   Many examples occur in industry in which high frequency sound propagates along a duct and then

78   radiates from the open end, causing annoyance to observers living in close proximity. Particular examples

79   include the noise propagating along a modern turbofan aeroengine, the sound field propagating up large

80   chimney stacks and the noise propagating along ventilation duct systems. A particular characteristic of these

81   broadband sound fields is that, at sufficiently high frequency, they comprise numerous propagating duct

82   modes, each of which has different amplitudes and phase speed. Knowledge of the pressure modal amplitudes

83   is important in the design of an effective sound absorbing liner for determining the sound power transmitted

84   along the duct and the far field radiation directivity pattern. However, as frequency increases the number of

85   modes that can propagate along the duct increases roughly as the square of the frequency. In large ducts

86   therefore, even at quite moderate frequencies, the number of duct modes that are able to propagate can

87   readily exceed several hundred.

88

89   One of the first attempts at determining mode amplitudes from measured acoustic pressure data in a duct

90   was by Moore[2] who describes a method for determining the circumferential and radial modes at the inlet of a

91   duct. A similar principle is described by Thomas et al[3], which then extended by extended by Farassat, Nark,

92   and Russel[4] . Their approach consists in applying Fourier analysis of the far-field pressure in the azimuthal

93   direction to deduce the spinning mode amplitudes. The radial modes within each spinning mode were

94   deduced by inverting a system of linear equations relating the pressure measurements to the mode

95   amplitudes. The conditioning of the matrix to be inverted was assessed and some regularisation techniques

96   applied to reduce the errors introduced by the poorly conditioned matrix. However, their technique requires

97   roughly twice the total number of propagating modes to be inverted and is restricted to tonal noise. Since

98   these early papers there have been numerous variants on this approach for deducing the mode amplitudes at

99   a single frequency, such as that proposed by Lewy[5] for deducing the far field radiation.

100

101   Relatively few measurement techniques for the detection of mode amplitudes of the broadband sound

102   field can be found in the literature, in which the acoustic signal is distributed over a frequency bandwidth and

103   whose mode amplitudes are generally uncorrelated. Two such techniques have been presented by Enghardt

104   et al[5] and Tapken[6] that requires cross-spectral measurements to be made between a number of microphones

105   and a single reference microphone at the duct wall. However, a similar number of microphones are needed as

106   the methods proposed for single frequency radiation, which is prohibitively large at moderate to high

107   frequencies ($ka > 20$, where k is the free space wavenumber and a is the duct radius).

108

109   Another approach is that adopted by Abom[7] who uses a system of transfer function measurements made

110   between a number of microphone pairs in the duct. Again, as many measurements as modes are needed to

111   solve the full system of equations and determine all mode amplitudes.

112

113   Lowis et al[8] have proposed a pragmatic approach to determining the mode amplitude distribution. It is based

114   on the hypothesis that different modes with the same propagation angle have similar sound transmission and

115   radiation characteristics. It is therefore sufficient to determine the modal amplitudes as a function of

116   propagation angle modes rather than the usual mode indices (m,n). The approach by Lowis et al uses an axial

117   array of equally spaced microphones along the duct wall to perform beamforming of the acoustic pressure at

118   the duct to to estimate the in-duct noise directivity. This in-duct directivity may then be used to infer the far

119   field directivity.

120

121   Rather than providing information about the mode amplitude for the different mode orders (m,n), the

122   technique provides information about the distribution of mode amplitudes versus in-duct propagation angle.

123   For the intended applications listed above, this limitation presents no difficulty as it has long been recognized

124   that modes with the same propagation angles possess near identical transmission and radiation

125   characteristics[9].

126

127   **II. MODAL TRANSMISSION**

128

129   Consider a hard-walled cylindrical duct of finite-length, as sketched in Fig 1 below, containing an axial

130   uniform mean flow moving in the positive x direction with flow speed cM ($M > 0$), where c is the sound speed

131   and M is the mean flow Mach number. A point on the duct cross section is represented by $\mathbf{y} = (r,\theta)$ and x

132   denotes the axial distance along the duct relative to some arbitrary origin. Two microphones mounted flush

133   to the duct wall, separated axially by a distance Δx, are used to detect the acoustic pressure. The objective

134   here is to deduce the distribution of mode amplitudes in the duct using the acoustic pressure information at
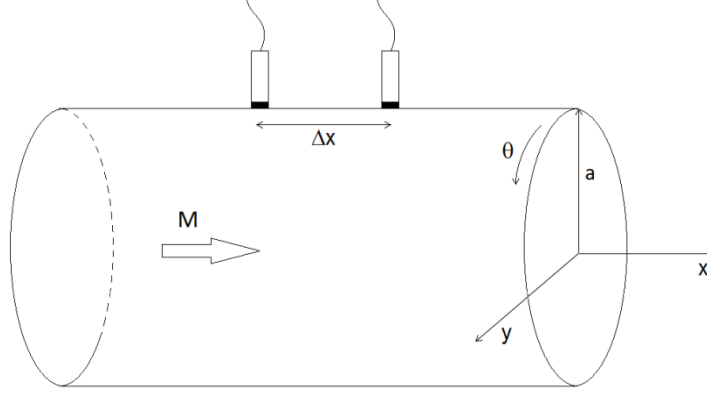
135   the two microphones.

4

136

137

Figure 1. Semi-infinite, hard walled unflanged circular duct with associated co-ordinate system. Two microphones mounted flush to the duct wall, separated axially by a distance Δx, are used to detect the acoustic pressure.

The sound field $p(x,\mathbf{y})$ in the duct satisfies the convected homogeneous wave equation,

$$\left(\frac{1}{c^2} \frac{\overline{D}^2}{Dt^2} - \nabla^2 \right) p = 0 \tag{1}$$

where $\dfrac{\overline{D}}{Dt} = \dfrac{\partial}{\partial t} + c\, M\, \dfrac{\partial}{\partial x}$ is the convected derivative operator associated with the mean flow velocity

$(cM,0,0)$ in the $(x,\mathbf{y})$ coordinate system and c is the sound speed in the quiescent medium. Above its cutoff

frequency, at a single frequency ω, a single mode of pressure amplitude A_{mn} is described by

$$p_{mn}^{\pm}(\mathbf{y},x) = e^{-i\omega t} A_{mn}^{\pm} \Psi_{mn}(\mathbf{y}) e^{ik_{mn}^{\pm}x} \tag{2}$$

where the superscript '+; refers to modes propagating in the direction of flow and '-' to modes propagating in

the opposite direction to the flow. Equation (2) in Eq. (1) gives

156
$$k_{mn}^{\pm} = \left(\frac{\alpha_{mn}^{\pm} - M}{\beta^2} \right) \frac{\omega}{c}, \quad \alpha_{mn}^{\pm} = \pm\sqrt{1 - \left(\kappa_{mn}/k \right)^2 \beta^2} \; . \tag{3a,b}$$

157

158   where $\beta^2 = \left(1 - M^2 \right)$, $k = \omega/c$ where ω is the angular frequency and c the speed of sound, and κ_{mn} are a set of

159   eigenvalues that are characteristic of the duct cross section such that the corresponding mode shape

160   functions Ψ_{mn}, defined by $\left(\nabla_{\perp}^2 + \kappa_{mn}^2 \right) \Psi_{mn}(\mathbf{y}) = 0$, also satisfy the duct-wall boundary conditions and the

161   normalization condition $A^{-1} \int_A \left| \Psi_{mn}(\mathbf{y}) \right|^2 dA(\mathbf{y}) = 1$. The parameter $\alpha_{mn}^{\pm}$, which we shall call the cut-on ratio, is

162   central in what follows, and takes values between $\alpha_{mn}^{\pm} = 0$ precisely at the modal cutoff frequency

163    $\omega = \omega_{mn} = \kappa_{mn} c \left(1 - M^2 \right)^{-\frac{1}{2}}$, and tends to $\left| \alpha_{mn}^{\pm} \right| = 1$ as $\omega/\omega_{mn} \to \infty$, corresponding to modes well above cuton.

164

165   To simplify the notation the superscripts + and – on α are now dropped and it is now understood that modes

166   propagating in the direction of the flow are represented by $\alpha_{mn} \geq 0$ while modes propagating in the opposite

167   direction (against the flow) are represented by $\alpha_{mn} \leq 0$.

168

169   The in-duct sound field at any position in the duct cross section $\mathbf{y} = (r, \theta)$, axial position x, and frequency ω,

170   can be expressed as the sum of modal components propagating in the direction of flow p_{mn}^{+}, and modes

171   propagating opposite to the direction of flow p_{mn}^{-},

172

173
$$p(\mathbf{y}, x) = \sum_{m=-\infty}^{\infty} \sum_{n=0}^{\infty} \left[p_{mn}^{+}(\mathbf{y}, x) + p_{mn}^{-}(\mathbf{y}, x) \right], \tag{4}$$

174

175   where (m,n) are the usual circumferential and radial mode indices[9].

176

III. ACOUSTIC PRESSURE AT THE DUCT WALL

The acoustic pressure cross spectrum between two points separated axially along the duct wall $\mathbf{y}_a = (r = a, \theta)$, at axial distances x_1 and $x_1 + \Delta x$, may written as,

$$S_{12}(\omega, \mathbf{y}_a, x_1, x_2) = \frac{\pi}{T} E\{p(\mathbf{y}_a, x_1) p^*(\mathbf{y}_a, x_1 + \Delta x)\} \tag{5}$$

where $E\{\}$ denotes the expectation and the acoustic pressures refer to Fourier Transforms of the pressure time series taken over a time duration T. For incoherent excitation of the sound field we treat the mode amplitudes as uncorrelated random variables so that $E\{A_{mn} A_{m'n'}^*\} = 0$. We further assume that the incident and reflected pressure will be incoherent since each mode will reflect with a different phase shift and hence, $E\left\{\sum_{m,n}\left[A_{mn}^+(\omega) A_{mn}^{-*}(\omega)\right]\right\} = 0$. Substituting Eqs (2) and (4) into Eqs (5) and invoking the uncorrelated incident and reflected pressure assumption above leads to,

$$S_{12}(\omega, \mathbf{y}) = \sum_{m,n}\left[E\left\{\left|A_{mn}^+(\omega)\right|^2\right\} e^{ik_{mn}^+ \Delta x} + E\left\{\left|A_{mn}^-(\omega)\right|^2\right\} e^{ik_{mn}^- \Delta x}\right]\Psi_{mn}^2(\mathbf{y}) \tag{6}$$

Work by Rice[9], and more recent work by Joseph et al[10], have shown that there are a physically important class of source distributions for which the *relative* mode amplitude distribution is *independent* of frequency and only a function of the cut off ratio α_{mn} (equivalently, mode propagation angle[9], see equation (25) below). Well known examples include a uniform distribution of monopole sources, axial dipole sources and equal energy per mode[10]. In these, and many other source distributions, we may write,

$$E\left\{\left|A_{mn}^\pm(\omega)\right|^2\right\} = S(\omega)\overline{a_\pm^2}(\alpha_{mn}) \tag{7}$$

7

200 where $S(\omega)$ is the frequency-dependent source strength with dimensions of pressure squared per unit

201 frequency and $\overline{a_\pm^2}(\alpha_{mn})$ specifies the relative distribution of non-dimensional mean square mode amplitudes,

202 which depends only on α_{mn}. A list of some physically important examples can be found in Joseph et al[10]. The

203 assumption of the separability of $E\left\{\left|A_{mn}^\pm(\omega)\right|^2\right\}$ into a purely frequency–dependent term $S(\omega)$ and a mode

204 distribution term $\overline{a_\pm^2}(\alpha_{mn})$ (which controls the spatial variation of the sound field) is central to the validity of

205 the technique. The split between the two terms in Eq. (7) is essentially arbitrary. For reasons that will become

206 clear below, we define $\overline{a_\pm^2}(\alpha_{mn})$ to have the normalization property,

207

208
$$\sum_{m,n}\left[\overline{a_+^2}(\alpha_{mn})+\overline{a_-^2}(\alpha_{mn})\right]=1 \tag{8}$$

209

210 We now denote the amplitude of waves propagating against the direction of flow (i.e., reflected modes in this

211 case) by negative argument α so that

212

213
$$\overline{a_+^2}(\alpha_{mn})=\overline{a^2}(\alpha_{mn}), \qquad \alpha_{mn}\geq 0$$
$$\overline{a_-^2}(-\alpha_{mn})=\overline{a^2}(\alpha_{mn}), \qquad \alpha_{mn}\leq 0 \tag{9}$$

214

215 In the high frequency limit ($ka = \omega a/c > 10$ has been found to be sufficient from our simulations, where a is

216 the duct radius), we may treat $\overline{a^2}(\alpha)$ as a continuous variable so that the discrete summation over $\overline{a^2}(\alpha_{mn})$

217 in Eq. (6) may be replaced by an integration over α. The normalization condition of Eq. (8) may therefore be

218 written as

219

220
$$\int_{-1}^{1}\overline{a^2}(\alpha)n(\alpha)d\alpha =1 \tag{10}$$

221

222   where $n(\alpha)$ the modal density function introduced to take into account the distribution of modes across their

223   range of α- values, defined by,

224

225 $$n(\alpha) = \frac{N(\alpha + \delta\alpha) - N(\alpha)}{N\delta\alpha}\bigg|_{\lim \delta\alpha \to 0} , \quad \int_{-1}^{1} n(\alpha)d\alpha = 1 \qquad (11a,b)$$

226

227   where $N(\alpha)$ is the number of modes with 'α' values of between -1 and α and N is the total number of

228   propagating modes at frequency ka, i.e., $N = N(1) = \int_{-1}^{1} N(\alpha)d\alpha$. Rice has shown that in a cylindrical duct with

229   uniform mean flow, the total number of propagating modes N takes the high-frequency limiting value[9],

230

231 $$N \to \left(\tfrac{1}{2}ka/\beta\right)^2, \qquad ka/\beta \to \infty \qquad (12)$$

232

233   Following Rice[9], and re-expressed in terms of cuton ratio α by Joseph et al[10,11], the high-ka asymptotic density

234   function n, is given by,

235

236 $$n(\alpha) = |\alpha| \qquad (13)$$

237

238   Note that Eq. (13) differs by a factor of ½ from the expression originally presented by Joseph et al[10], which

239   assumes a distribution a modes propagating from *one direction* only. Equation (13) indicates a scarcity of

240   modes that are just cut-on ($\alpha \approx 0$) compared with a higher population of modes that are well cut on, ($|\alpha| \approx 1$).

241

242   Simplifications to Eq. (6) for the pressure cross spectrum at the duct wall are obtained by replacing $\Psi_{mn}^2(\mathbf{y})$

243   by its average value at the duct wall[10], averaged over all values of mode indices m and n,

244

245 $$\Psi_{mn}^2(\mathbf{y}) = \left\langle \Psi^2(\mathbf{y}) \right\rangle_{mn} = 2 \,. \tag{14}$$

246

247 Taking the average incurs greatest error for modes with the largest m values whose values of $\Psi_{mn}^2(\mathbf{y})$ are

248 concentrated at the duct wall. These modes are comparatively scarce, however (with $m = 0$ having the largest

249 number of radial modes and hence being most common), and hence the approximation of Eq. (14) introduces

250 negligible error compared with the exact calculation of Eq. (6). Substituting Eq. (7) for $\left|A_{mn}(\omega)\right|^2$, Eq. (3a) for

251 k_{mn}, and taking the high frequency limit in the sense of Eq. (10), leads to an integral expression for the

252 pressure cross spectrum $S_{12}(\omega, \mathbf{y}_a, \Delta x)$ between two microphones separated axially by a distance Δx at the

253 duct wall $\mathbf{y}_a = (a, \theta)$ involving only the cutoff ratio and the frequency-dependent source strength,

254

255 $$\frac{S_{12}(\hat{\omega}, \mathbf{y}_a)}{S(\hat{\omega})} = 2\mathrm{Ne}^{-iM\hat{\omega}} \int_{-1}^{1} \overline{a^2}(\alpha) n(\alpha) e^{i\hat{\omega}\alpha} d\alpha \,, \tag{15}$$

256

257 which is a function only of the non-dimensional frequency, $\hat{\omega}$

258

259 $$\hat{\omega} = \omega \Delta x / c\beta^2 \,, \tag{16}$$

260

261 Note that the source term $S = S(\hat{\omega})$ has also been written as a function of $\hat{\omega}$ which is permissible since S is a

262 source term and therefore unrelated to Δx and so there is no difficulty in non-dimensionalising the source

263 frequency ω with respect to this arbitrary distance.

264

265 A consequence of making the separability assumption of Eq. (7) is that the cross spectrum is only a function

266 of the non-dimensional frequency, $\hat{\omega}$. Thus, cross spectra measured at the duct wall for different separation

267 distances Δx, plotted against $\hat{\omega}$, should collapse provided that this separability assumption is met. This

268 property therefore provides a simple test of the validity of Eq. (7). In practice, however, the coherence

269 measurement will be affected by non-acoustic pressure contributions from flow noise at the microphones. In

10

270   practice, therefore, steps should be taken to minimize contamination by flow noise by, for example, recessing

271   the microphones into the duct wall.

272

273   A. Interpretation of S.

274   Putting $\Delta x = 0$ in Eq (6) yields the pressure Power Spectral Density $S_{11}(\omega, \mathbf{y})$ at *any* point over the duct cross

275   section $\mathbf{y}$. Averaging the result over the duct cross section area A and taking the high frequency limit yields,

276

277
$$\left[\frac{1}{A} \int_S S_{11}(\hat{\omega}, \mathbf{y}) dS(\mathbf{y}) \right]_{f \to \infty} = S(\hat{\omega}) \mathrm{N} \left[\int_{-1}^{1} \overline{a^2}(\alpha) n(\alpha) d\alpha \right] \left[\frac{1}{A} \int_A \Psi_{mn}^2(\mathbf{y}) dS(\mathbf{y}) \right] \tag{17}$$

278

279   Noting the normalization property of the mode shape functions, $A^{-1} \int_S \Psi_{mn}^2(\mathbf{y}) dS(\mathbf{y}) = 1$ and the mode

280   amplitude normalization property of Eq. (10), Eq. (17) reduces to,

281

282
$$S(\hat{\omega}) = \left[\frac{1}{\mathrm{N}} \frac{1}{A} \int_S S_{11}(\hat{\omega}, \mathbf{y}) dS(\mathbf{y}) \right]_{f \to \infty} \tag{18}$$

283

284   The source strength $S(\hat{\omega})$ therefore has the interpretation as the high frequency noise pressure spectrum

285   averaged over the duct cross sectional area, per mode. Joseph et al[10] have shown that, in the high frequency

286   limit, the pressure PSD averaged over the duct cross section, $\mathrm{N}S(\hat{\omega})$, is half the pressure Power Spectral

287   Density (PSD) measured at the duct wall $S_{11}(\hat{\omega}, \mathbf{y}_a)$, i.e.,

288

289    $S_{11}(\hat{\omega}, \mathbf{y}_a) = 2\mathrm{N}S(\hat{\omega})$ (19)

290

291   Substituting Eq. (19) into (15) leads to,

292

293
$$S_{12}(\hat{\omega}) = S_{11}(\hat{\omega}) e^{-iM\hat{\omega}} \int_{-1}^{1} \overline{a^2}(\alpha)|\alpha| e^{i\hat{\omega}\alpha} d\alpha \qquad (20)$$

294

295 In Eq. (20), and all future results, the dependence on $\mathbf{y}_a$ is dropped since it is now understood that *all*

296 measurements are made at the duct wall.

297

298 The approximation is now made that $S_{11}(\hat{\omega}) \approx S_{22}(\hat{\omega})$ and hence $S_{11}(\hat{\omega}) \approx \sqrt{S_{11}(\hat{\omega})S_{22}(\hat{\omega})}$, since Δx is usually very

299 small compared to the acoustic wavelength (typically a few centimeters). Finally the limits of integration of

300 Eq. (20) are now extended to $\pm\infty$ based on the principle that modes for which $|\alpha| > 1$ are not defined, do not

301 exist, and may therefore be set equal to zero $\overline{a^2}(\alpha) = 0$ for α – values in this range. The final result is,

302

303
$$\psi_{12}(\hat{\omega}) = e^{-iM\hat{\omega}} \int_{-\infty}^{\infty} \overline{a^2}(\alpha)|\alpha| e^{i\hat{\omega}\alpha} d\alpha \qquad (21)$$

304

305 Equation (21) represents a Fourier Transform relationship between the α – weighted normalized mode

306 amplitude distribution function $\overline{a^2}(\alpha)$ and the complex coherence function $\psi_{12}(\hat{\omega})$,

307

308
$$\psi_{12}(\hat{\omega}) \approx \frac{S_{12}(\hat{\omega})}{\sqrt{S_{11}(\hat{\omega})S_{22}(\hat{\omega})}} \quad (0 \le |\psi_{12}(\hat{\omega})|^2 \le 1) \qquad (22)$$

309

310 The mean square mode amplitude distribution, with the normalization property of Eq (8), may therefore be

311 readily deduced from the inverse Fourier Transform of the complex coherence function, weighted by $e^{iM\hat{\omega}}$.

312

313
$$\overline{a^2}(\alpha) = \frac{1}{2\pi|\alpha|} \int_{-\infty}^{\infty} \psi_{12}(\hat{\omega}) e^{iM\hat{\omega}} e^{-i\hat{\omega}\alpha} d\hat{\omega} \qquad (23)$$

314

315   Equation (23) is the main result of this paper. It suggests that the normalized mode amplitude distribution

316   may in principle be deduced using just two microphones for any incoherent multi-mode sound field whose

317   mode amplitude distribution satisfies the separability condition of Eq. (7). The phase factor $e^{iM\hat{\omega}}$ serves as a

318   Lorentz transformation into the reference frame moving with the flow such that the amplitude distribution

319   for right and left-traveling propagating modes is now symmetric in α, lying in the range $-1 \geq \alpha > 1$.

320

321   B. Fourier Relationships

322   Equations (21) and (23) are the main results of this paper. They suggest that modal cuton ratio and flow-

323   corrected Helmholtz number, $[\alpha, \hat{\omega}]$, are conjugate variables which form *Fourier transform* pairs in the same

324   way that, for example, time and frequency, [*t, f*] are related. It is therefore not possible to specify both

325   quantities simultaneously with arbitrary precision. By specifying certainty in the frequency spectrum and

326   hence small values of $\Delta\hat{\omega}$, by for example imposing high resolution in the frequency spectrum, therefore

327   imposes corresponding uncertainly $\Delta\alpha$ (or poor resolution) in the α - spectrum, $\Delta\alpha = 2\pi/\Delta\hat{\omega}$.

328

329   The α – spectrum is bounded by $0 \leq |\alpha| \leq 1$, with values $|\alpha| > 1$ representing cutoff modes whose amplitude

330   decay exponentially away from the source. The bandwidth $\Delta\alpha$ (appropriately defined) must therefore be

331   less than unity and hence the coherence bandwidth (defined in a consistent way with $\Delta\alpha$) satisfies and hence

332   $\Delta\hat{\omega}\Delta\alpha \approx 2\pi$. A consequence of this band-limited behavior is that bandwidth of the coherence function is also

333   bounded by $\Delta\hat{\omega} \approx 2\pi$.

334

335   C. Directivity

336   In this section we explore how the two microphone method may be used to deduce the far field mean square

337   pressure directivity $S_{ff}(\omega, \theta)$. Sinayoko et al[12] have recently shown that, for the idealized case where the flow

338   speed is uniform and *everywhere the same*, in the high frequency limit, there is a direct correspondence

339   between the mean square modal distribution *incident* upon the open end of the duct $\overline{A_+^2}(\alpha)$ and the far field

340 directivity. Putting Eq. (7), $E\left\{\left|A_{mn}^{+}(\omega)\right|^{2}\right\}=\frac{1}{2}S_{11}(\omega)\overline{a_{+}^{2}}(\alpha_{mn})$, in Eq. (26) of the paper by Sinayoko et al[12], this

341 expression may be written as

342

343
$$\frac{S_{ff}(\omega,\theta)}{S_{11}(\omega)}=\frac{1}{4}\left(\frac{a}{R}\right)^{2}\frac{\beta^{2}\cos^{2}\theta}{1-M^{2}\sin^{2}\theta}\overline{a_{+}^{2}}(\alpha) \tag{24}$$

344

345 where α is related to far field polar radiation angle θ relative to the duct axis by[9],

346

347
$$\alpha(\theta)=\frac{\cos\theta}{\sqrt{1-M^{2}\sin^{2}\theta}} \qquad (0\le\theta\le\pi/2) \tag{25}$$

348

349 Substituting Eq. (23) for $\overline{a_{+}^{2}}(\alpha)$ in Eq. (24), the final result for the pressure PSD directivity $S_{ff}^{\pm}(\omega,\theta)$ in terms

350 of the complex coherence function $\psi_{12}(\hat{\omega})$ for the case where the flow speed is everywhere the same is

351

352
$$\frac{S_{ff}(\omega,\theta)}{S_{11}(\omega)}=\frac{1}{8\pi}\left(\frac{a}{R}\right)^{2}\frac{\cos\theta}{\sqrt{1-M^{2}\sin^{2}\theta}}\int_{-\infty}^{\infty}\psi_{12}(\hat{\omega})e^{iM\hat{\omega}}e^{-i\hat{\omega}\cos\theta/\sqrt{1-M^{2}\sin^{2}\theta}}\,d\hat{\omega} \qquad (0\le\theta\le\pi/2) \tag{26}$$

353

354 Predictions of the far field directivity $S_{ff}(\omega,\theta)$ deduced from measurements of the acoustic pressure coherence

355 function $\psi_{12}(\hat{\omega})$ have been presented in a recent paper by Melling et al[13]. In this work, one end of a plastic duct of

356 length 4.34m and internal dimeter 0.4m was located within a reverberation chamber which was excited by four

357 loudspeakers excited by incoherent white noise signals. The other end of the pipe was located within an anechoic

358 chamber to allow measurements of the far field directivity function using 11 equally spaced microphones along an

359 arc, 2.5m from the duct center. These direct directivity measurements were compared at the frequencies of 3kHz,

360 6kHz and 12kHz against directivity estimates deduced from the pressure coherence function at the duct wall from

361 two microphones separated at various distances. Agreement between the directly measured directivity and the

362   estimated directivity from Eq. (26) from measurements of the coherence function are generally within about 5dB at

363   any given frequency and radiation angle

364   **IV.   SOUND POWER**

365   The total sound power flowing along the duct provides a single measure of total noise generation. Its exact

366   measurement in a duct system requires the amplitude of individual modes to be determined in both

367   directions, which requires numerous microphone measurements. Alternatively, total power transmission can

368   be determined from the integration of the far field intensity from the duct inlet or exhaust. In this section we

369   show how upstream and downstream sound power in the mean flow can be determined solely from the

370   complex coherenct function at the duct wall.

371

372   In a duct with uniform mean flow the sound power transmitted along the duct is the sum of the incident and

373   reflected sound powers,

374

375    $$W(\omega) = W^+(\omega) + W^-(\omega) \tag{27}$$

376

377   The sound power in each direction may be computed from the sum of their respective modal power

378   components[14],

379

380    $$W^\pm(\omega) = \sum_{m,n} W_{mn}^\pm(\omega), \quad W_{mn}^\pm(\omega) = \frac{\pm\alpha_{mn} A |A_{mn}^\pm|^2}{2\rho c} \frac{(1-M^2)^2}{(1\mp\alpha_{mn}M)^2} \quad (\alpha_{mn} \geq 0) \tag{28a,b}$$

381

382   Taking the high frequency limit, substituting Eq. (7) for $|A_{mn}|^2$ and Eq. (13) for $n(\alpha)$, noting that

383    $S(\omega) = \frac{1}{2}S_{11}(\omega, \mathbf{y})$, and representing negative going modes by negative α as in Eq. (20), yields the following

384   expression for the normalized sound power spectrum transmitted along the duct in the direction of flow,

385    $W^+(\omega)$ and against the flow $W^-(\omega)$ of the form,

386

387
$$\frac{4\pi W^{\pm}(\omega)\rho c}{S_{11}(\omega)\beta^4 A} = \int_0^\infty \psi_{12}(\hat{\omega})\Omega^{\pm}(\hat{\omega}, M)e^{iM\hat{\omega}}d\hat{\omega}$$
(29)

388   where

389

390
$$\Omega^-(\hat{\omega}, M) = \int_{-1}^0 \frac{\alpha e^{i\hat{\omega}\alpha}}{(1-\alpha M)^2}d\alpha, \quad \Omega^+(\hat{\omega}, M) = \int_0^1 \frac{\alpha e^{i\hat{\omega}\alpha}}{(1-\alpha M)^2}d\alpha$$
(30a,b)

391

392   These power factors may be evaluated in terms of standard functions,

393

394
$$\Omega^{\pm}(\hat{\omega}) = \frac{e^{i\hat{\omega}/M}}{M^3}\left[\mp(M+i\hat{\omega})Ei\left(\frac{-i\hat{\omega}}{M}\right)\mp Me^{-i\hat{\omega}/M} \pm (M+i\hat{\omega})Ei\left(\frac{i\hat{\omega}(\pm M-1)}{M}\right) - \frac{M}{M\mp 1}e^{i\hat{\omega}(\pm M-1)/M}\right]$$
(31)

395

396   where $Ei(x)$ denotes the Exponential integral function, $Ei(x) = \int_{-\infty}^x (e^t/t)dt$. The final expression for the sound

397   power spectrum $W(\omega)$ normalized on the pressure PSD at the duct wall $S_{11}(\omega)$ may therefore be written in

398   the form of a single integral over non-dimensional frequency.

399

400   Equation (29) predicts that $W(\hat{\omega})\rho c / AS_{11}(\hat{\omega}) \propto f(M)$, i.e., that the ratio of sound power to mean square

401   pressure (at the duct wall) is a non-dimensional function of Mach number and is a frequency-independent

402   constant for the class of mode amplitude distribution functions of interest in this paper. This was also the

403   finding by Joseph et al[10] in exact calculations of $W(\hat{\omega})\rho c / S_{11}(\hat{\omega})A$ for a variety of mode amplitude

404   distributions, which allowed sound power to be deduced from measurements of the pressure spectrum at the

405   duct wall providing the mode amplitude distribution was known *a priori*. The current method allows this

406   constant to be determined from the coherence function which provides information about the mode

407   amplitude distribution.

408

409   An alternative expression for the transmitted sound power may be obtained by integrating the far field

410   intensity over a hemi-sphere with the assumption that, (*i*) the sound power incident upon the duct exit is

16

411   radiated to the far field, (*ii*) most of the sound power is transmitted between polar angles in the range

412    $0 \leq \theta \leq \pi/2$, i.e., with negligible radiation to the rear arc. The PSD of the radiated sound power may be

413   written in the form[6]

414

415
$$W(\omega) = \frac{4\pi R^2}{\rho c} \int\limits_0^{\pi/2} S_{ff}(\omega,\theta) F(\theta) \sin\theta d\theta \tag{32}$$

416

417   where R is the distance from the duct centre at which S_{ff} is evaluated and,

418

419
$$F(\theta) = \frac{\beta^4 \sqrt{1 - M^2 \sin^2\theta}}{2\left(\sqrt{1 - M^2 \sin^2\theta} - M\cos\theta\right)^2} \tag{33}$$

420

421   Substituting Eq. (26) into (32) gives an alternative expression for the radiated sound power, which unlike Eq.

422   (29), involves a double integration over ω and θ,

423

424
$$\frac{W\rho c}{S_{11}(\omega)a^2} = \frac{\beta^4}{16}\left(\frac{ka}{2}\right)^2 \int\limits_0^{\pi/2} \Theta(\theta) \int\limits_{-\infty}^{\infty} \psi_{12}(\hat{\omega}) e^{iM\hat{\omega}} e^{-i\hat{\omega}\cos\theta/\sqrt{1-M^2\sin^2\theta}} d\hat{\omega} d\theta \tag{34}$$

425   where

426

427
$$\Theta(\theta) = \frac{\cos\theta\left(1 - M^2 \sin^2\theta\right)}{\left(1 - M^2 \cos^2\theta\right)\left(\sqrt{1 - M^2 \sin^2\theta} - M\cos\theta\right)^2} \tag{35}$$

428   **V. NUMERICAL VALIDATION AND SPECIAL CASES**

429   In this section we validate the principles set out above by a number of numerical examples to illustrate the

430   effectiveness of the technique in deducing, based only on the complex coherence measurement at the duct

431   wall, the mode amplitude distribution and transmitted sound power for incident and reflected modes, and the

432   far field pressure directivity. Further, we consider in detail some special idealized cases for more detailed

433   analysis.

434

435   We consider the idealized case of a duct in which all the modes propagating towards the end of the duct

436   contain equal sound power. The normalized mode amplitude distribution is obtained by setting $W_{mn}^{\pm}(\omega)=1$

437   in Eq. (28) and normalizing the result according to Eq. (11b),

438

439    $$\overline{a^2}(\alpha)=\frac{(1-\alpha M)^2}{\alpha(1+M^2/3)} \tag{36}$$

440

441   In a hard walled cylindrical duct the mode shape function are of the form $|\Psi_{mn}(r)|=|J_m(k_{r_{mn}}r)|/\Gamma_{mn}$, where J_m

442   are Bessel functions of the 1st kind or order m, $k_{r_{mn}}a$ is the nth stationary value of J_m and Γ_{mn} are constants

443   chosen to satisfy the normalisation condition presented above. Modal pressure reflection coefficients of the

444   form $R(\alpha)=\exp(-\delta\alpha/2)$ are assumed in the simulations, so that $\overline{a_-^2}(\alpha)=R^2(\alpha)\overline{a_+^2}(\alpha)$, where δ specifies the

445   rate at which the reflection coefficient diminishes as the modes is excited well above cut off. This reflection

446   coefficient model is consistent with other more accurate models and is designed to ensure that modes at

447   cutoff, $\alpha=0$, are perfectly reflected, with the reflection coefficient reducing as the modes become increasing

448   cuton as frequency is increased[14].

449

450   A. Special cases; zero Mach number, arbitrary reflection

451   We first consider the case of $M=0$ since it allows analytic expression to be derived and compared against

452   exact numerical predictions. For the case of Equal energy per Mode, the mode amplitude distribution may be

453   obtained by setting the sound power in each mode equal to unity, $W_{mn}^+(\omega)=W_0=1$ in Eq. (28),

454

455    $$\overline{a^2}(\alpha)=\begin{cases}1/\alpha N & \alpha\geq0\\ \exp(-\delta\alpha)/(|\alpha|N) & \alpha\leq0\end{cases} \tag{37}$$

456

457   where N is the factor designed to ensure that $\overline{a^2}(\alpha)$ is correctly normalized according to Eq. (10) and equals,

458    $N = \left(1 + \delta - e^{-\delta}\right)/\delta$.

459

460   B. Coherence function

461   The complex coherence function is obtained from substituting Eqs (37) into (21) to give

462

463    $$\psi_{12}(\hat{\omega}) = \frac{\delta}{1 + \delta - e^{-\delta}}\left[\frac{e^{-\delta/2}e^{-\frac{1}{2}i\hat{\omega}}\left[\sin\frac{1}{2}\hat{\omega}\cosh\frac{1}{2}\delta - i\cos\frac{1}{2}\hat{\omega}\sinh\frac{1}{2}\delta\right]}{\frac{1}{2}(\hat{\omega} - i\delta)} + \frac{e^{\frac{1}{2}i\hat{\omega}}\sin\left(\frac{1}{2}\hat{\omega}\right)}{\frac{1}{2}\hat{\omega}}\right]$$ (38)

464

465   Figures 2a and 2b show a comparison of the coherence magnitude and phase respectively, evaluated at the

466   duct wall for an equal energy per mode sound field computed from the exact modal summation of Eqs. (6 and

467   22) (solid curve) with the analytic expression of Eq. (38) (dashed curve). Comparison are shown for the four

468   reflection factors, δ = 0, 1, 2 and 5. Note that the curves have been separated for ease of readability.

469

470
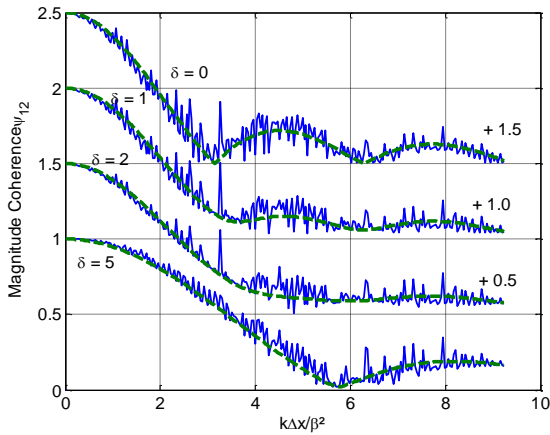
Figure 2a. Comparison of 'exact' and theoretical coherence function magnitude for $M = 0$ at different levels of reflectivity, δ = 0, 1, 2 and 5. Note that the curves have been separated for ease of viewing.
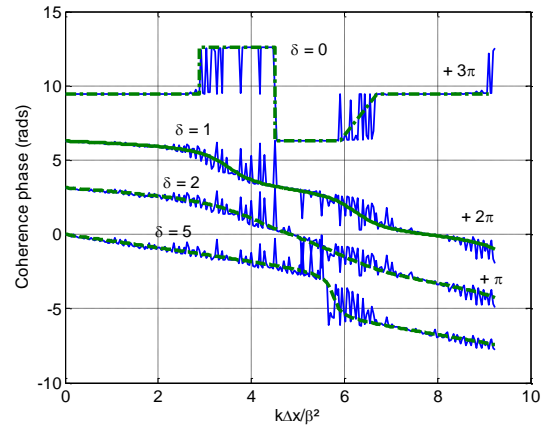
Figure 2b. Comparison of 'exact' and theoretical coherence function phase for $M = 0$ at different levels of reflectivity, δ = 0, 1, 2 and 5. Note that the curves have been separated for ease of viewing.

471

472   Oscillations in the exact calculation arise from the behavior of the spectra at the modal cuton frequencies.

473   Here the pressure amplitude tends to infinity as the cutoff frequency is approached. As the modal reflectivity

474   is increased (by reducing δ) the coherence magnitude and phase both exhibit greater variability.

475

476   Limiting cases of the coherence function may be obtained for the case of perfect modal reflectivity $\delta=0$, and

477   when the reflectivity is zero, i.e., the duct may be assumed to be infinite. In the latter case, putting $\delta \to \infty$ into

478   Eq. (38) yields

479

480   $$\psi_{12}(\hat{\omega}) \to \exp\left(\tfrac{1}{2} i \hat{\omega}\right) \frac{\sin\left(\tfrac{1}{2}\hat{\omega}\right)}{\tfrac{1}{2}\hat{\omega}} \tag{39}$$

481

482   which is in close agreeement with the exact calculation shown in figures 2a and 2b. The ducted sound field

483   may now be regarded as a one-sided (or hemi-diffuse sound field). The phase delay between the two

484   microphones which varies with frequency as $\tfrac{1}{2}\omega\Delta x/c$, i.e., precisely half the rate of a purely plane wave.

485   Precisely this behavior is observed in figure 2a and b for the case of least reflectivity, $\delta = 5$.

486

487   When all modes are perectly reflected at the end of the duct, $\delta \to 0$, and Eq. (38) tends to

488

489   $$\psi_{12}(\hat{\omega}) \to \frac{\sin \hat{\omega}}{\hat{\omega}} \tag{40}$$

490

491   In this case, where each incident mode has equal sound power and is perfectly reflected incoherently, the

492   coherence function is identical to that of a diffuse sound field in which energy is arriving from all angles

493   equally. Clearly, therefore, there is no phase variation between the two microphones, as shown in figure 2b,

494   where 2π phase jumps can be observed due to unwrapping issues.

495

496   C. Mode amplitude distribution

497   Figure 3 shows a comparison of the exact mean square mode amplitude distribution versus α of Eq. (37) with

498   that deduced by inversion of the complex coherence functions plotted in figures 2 by the use of Eq. (23).
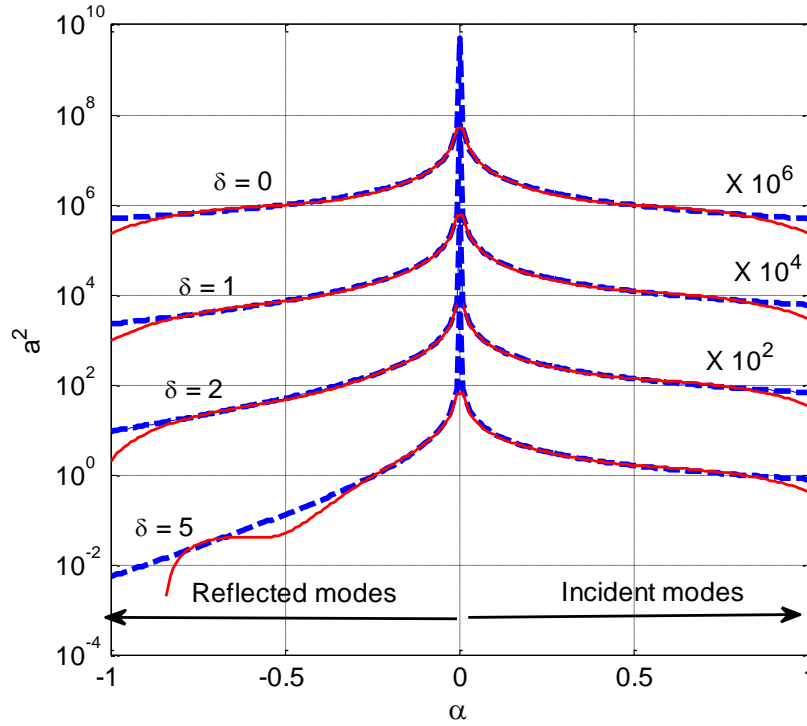

499

500   Figure 3. comparison of the exact (dashed curves) and inverted mode amplitude distribution (solid curves)
501   for four reflectivity factors at M = 0.
502

503   Agreement between the exact and inverted mode amplitude distribution is geneally excellent except near the

504   extreme value of α = 0, where the modes are well cuton, and $|\alpha| = 1$, corresponding to modes that are close to

505   cutoff. Errors are particularly great for the very well cuton modes. This is likely to be due to the choice of

506   'equal energy per mode' model chosen for the simulation since the mode distribution becomes singular at α =

507   0, which clearly cannot be recovered from Eq. (23) using a numerical integration. Errors are also pronounced

508   for the near-cutoff modes particularly for the case of least reflectivity arising from numerical errors in the

509   evaluation of Eq. (23).

510

511   D. Directivity

512   At zero Mach number, Eq. (26) for the normalised directivity becomes

21

513

$$\frac{S_{ff}(\omega,\theta)}{S_{11}(\omega)} = \frac{1}{8\pi}\left(\frac{a}{R}\right)^2 \cos\theta \int_{-\infty}^{\infty} \psi_{12}(\hat{\omega}) e^{-i\hat{\omega}\cos\theta} \, d\hat{\omega} \qquad (41)$$

515

516   Equation (39) in Eq. (41) yields the following expression for the radiated pressure

517

$$\frac{S_{ff}^{\pm}(\omega,\theta)}{S_{11}(\omega)} = \frac{1}{8\pi}\left(\frac{a}{R}\right)^2 \cos\theta \int_{-\infty}^{\infty} \frac{\sin\left(\frac{1}{2}\hat{\omega}\right)}{\frac{1}{2}\hat{\omega}} e^{-i\hat{\omega}\left(\cos\theta+\frac{1}{2}\right)} \, d\hat{\omega} \qquad (42)$$

519

520   The integral over $\hat{\omega}$ is independent of θ and equals 2π so that

521

$$\frac{S_{ff}^{\pm}(\omega,\theta)}{S_{11}(\omega)} = \frac{1}{4}(a/R)^2 \cos\theta \qquad (43)$$

523

524   A comparison of the exact directivity (solid curve) normalised on the pressure spectrum at the duct wall

525   evaluated at the maximum frequency of interest in this calculation with that deduced from the inversion of

526   the coherence (dashed curve) is shown below in figure 4 .

527
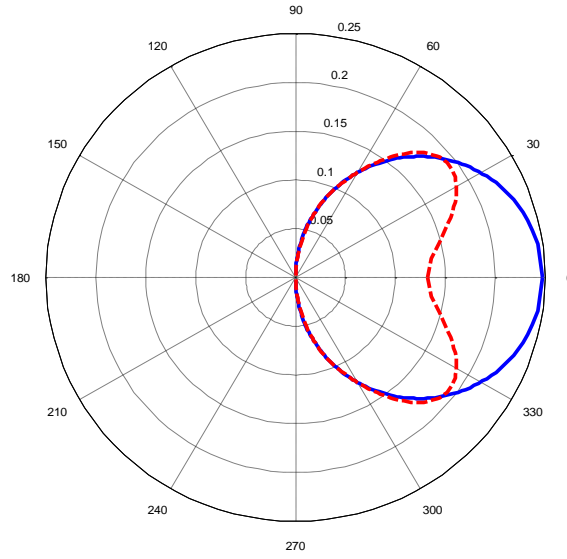
Figure 4. comparison of mean square pressure directivity at $M = 0$ for $\delta = 20$ obtained by inversion of the coherence function (dashed curve) and the theoretical directivity of Eq. (49) (solid curve).

Agreement is excellent at radiation angles beyond about $45°$ to the duct axis but then deviates at smaller

angles close to the duct axis, incurring a maximum error on-axis of about 40% in the pressure amplitude

(4.4dB in sound pressure level). Radiation within this range of angles is due to well cut-on modes with α –

values close to 1, as also observed in Fig 3 in which greatest error in the mode amplitude distribution is for α

~ 1, whose main radiation lobes are close to the duct axis. The reason for the error in these modes is due to

the Gibbs phenomenon in Fourier analysis, in which a 'ringing' type behaviour is observed in the vicinity of

piecewise discontinuities, such as in the present case. Here, the mode amplitude distribution is discontinuous

at $\alpha = 1$, since the measurement location is assumed to be well away from the source so that no cutoff modes

are present in the sound field, i.e., $\overline{a^2}(\alpha) = 0$ for $\alpha > 1$.

545   E. Sound Power

546   Figure 5a and 5b show the variation of upstream and downstream sound power versus $\hat{\omega}$ for the cases of

547   zero reflection (δ = 20) and perfect reflection, respectively. The dashed curve represents the variation

548   computed from the exact expression of Eq. (28) while the solid curve is that obtained by inversion of the
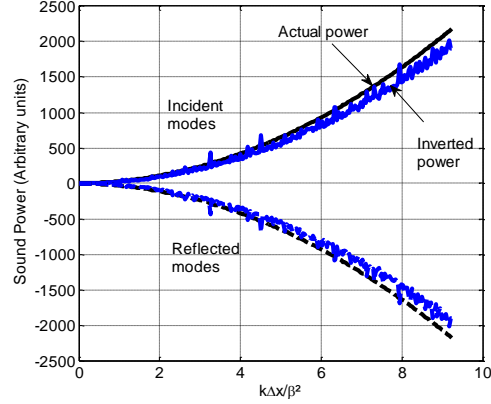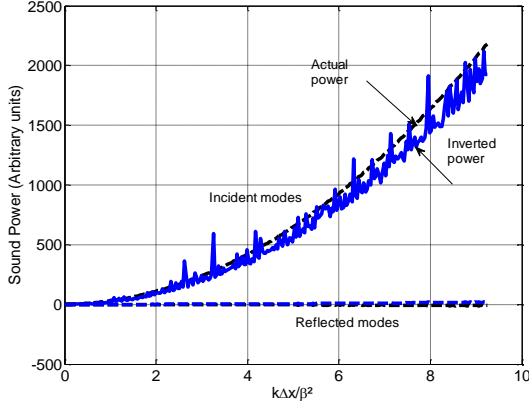
549   coherence function using Eq. (23).

550

Figure 5a. Comparison of actual (solid curve) and inverted (dashed curve) upstream and downstream sound power for $M = 0$ and $\delta = 20$.

Figure 5b. Comparison of actual (solid curve) and inverted (dashed curve) upstream and downstream sound power for $M = 0$ and $\delta = 0$.

551

552   Whilst this frequency variation is unrealistic since equal sound power per mode is assumed and each mode is

553   assumed to contain unit sound power the agreement observed above is useful for validating the

554   measurement principle. The power variation of the incident modes (before reflection) is therefore identical to

555   that of the variation of the number of modes. Thus, $W^+(\hat{\omega}) = \left(\frac{1}{2}ka\right)^2 W_0$, where $W_0 = 1$.

556

557   The general formulation for sound power in Eq. (29) may be evaluated exactly for the limiting case of zero

558   Mach number and reflectivity. In this case the power functions of Eq. (30) reduces to

559     $\Omega^+(\hat{\omega}) = \left[e^{i\hat{\omega}}(1 - i\hat{\omega}) - 1\right] / \hat{\omega}^2$. Substituting this and the coherence expression of Eq. (38) into (29) yields,

560

561
$$\frac{4\pi W^\pm(\omega)\rho c}{S_{11}(\omega)A} = \int_0^\infty \frac{e^{i\frac{1}{2}\hat{\omega}}\sin\left(\frac{1}{2}\hat{\omega}\right)}{\frac{1}{2}\hat{\omega}} \left[\frac{e^{i\hat{\omega}}(1 \mp i\hat{\omega}) \mp 1}{\hat{\omega}^2}\right] d\hat{\omega} \tag{44}$$

562

563

The integral on the right of Eq. (44) equals π and hence, the sound power transmitted along the duct and

hence radiated to the far field may be computed from,

$$W(\omega) = \frac{AS_{11}(\hat{\omega})}{4\rho c}, \tag{45}$$

This relationship between transmitted sound power and mean square pressure at the duct wall for the case of

an 'equal energy per mode' sound field has previously derived using an alternative method by Joseph et al[4].

F. Special cases: Perfect reflection ($\delta \to 0$), zero Mach number ($M \to 0$)

For completeness we consider the unrealistic case in which all propagating modes are reflected back into the

duct without attenuation.

For the case of the perfectly reflecting duct, substituting Eq. (40) for the coherence function into the

expression for sound power, Eq. (29), gives $W^{\pm}(\omega) \to 0$ and $S_{ff}(\omega,\theta) \to 0$. Thus, sound is perfectly reflected

from the open end and hence there is no net transmitted sound power and hence no far field radiation.

G. Special cases: Zero reflection ($\delta \to 0$), arbitrary Mach number

At moderately high frequency and above ($ka > 10$) modal reflections are weak except for all modes except

those excited close to their cut off frequency, where $|\alpha| \approx 1$. In this case we may set $\delta \to \infty$ and the

normalized mode amplitude distribution is given by Eq. (36). From Sinayoko et al[6] it may be shown that

$$S_{ff}(\theta) = \frac{1}{2}\left(\frac{2\rho c W_0}{A}\right)\left(\frac{a}{R}\right)^2\left(\frac{ka}{2}\right)^2 \frac{\left(\sqrt{(1-M^2\sin^2\theta)} - M\cos\theta\right)^2 \cos\theta}{\left(1+\frac{1}{3}M^2\right)\left(1-M^2\sin^2\theta\right)^{5/2}} \tag{47}$$

588   Putting (46) into (20) and taking the high frequency limit

589

590    $$S_{11} = 4\left(\tfrac{1}{2}ka/\beta\right)^2 2\rho c W_0 / A \tag{47}$$

591

592   So that the ratio of mean square far field pressure to that at the duct wall is

593

594    $$\frac{S_{ff}(\theta)}{S_{11}} = \frac{\beta^2}{4}\left(\frac{a}{R}\right)^2 \frac{\left(\sqrt{1-M^2\sin^2\theta}-M\cos\theta\right)^2 \cos\theta}{\left(1+\tfrac{1}{3}M^2\right)\left(1-M^2\sin^2\theta\right)^{5/2}} \tag{48}$$

595

596   This theoretical directivity function is compared against that obtained from the inversion of the complex

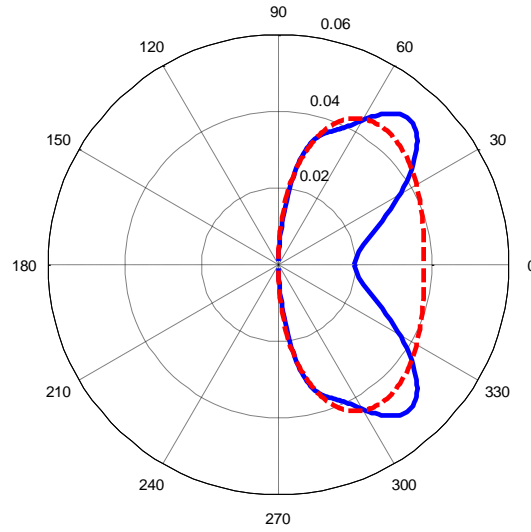597   coherence function calculated for $M = 0.5$ and $\delta = 20$ (not shown here) in figure 6.

598

599   Figure 6. comparison of mean square pressure directivity at $M = 0.5$ for $\delta = 20$ obtained by inversion of the
600   coherence function (solid curve) and the theoretical directivity of Eq. (49) (dashed curve)
601

602   As for the case of zero Mach number good agreement is observed at sideline angles with greatest incurred for

603   the angles close to the duct axis. The most pronounced effect of non-zero Mach number is that the directivity

604 is now 'flattened' with now most energy radiated to the sideline directions. This behavior is captured by the

605 inverted directivity function.

606

607 This relationship between transmitted sound power and the acoustic pressure PSD evaluated at the duct wall

608 for an equal energy per mode sound has been previously derived by Joseph et al[10] and provides a useful

609 estimate for the sound power in ducted broadband sound fields whose mode distribution is unknown.

610

611   H. Arbitrary Mach number and modal reflectivity

612 Finally, we present the coherence function and inverted mode amplitude distribution function for the case of

613 arbitrary Mach number and reflectivity. Figures 7a and b below show the coherence function for the more

614 general case of $M = 0.5$ and $\delta = 2$, where no analytic solution is available. The corresponding mode amplitude

615 distribution obtained from inversion of this coherence function using Eq. (23) compared with the exact

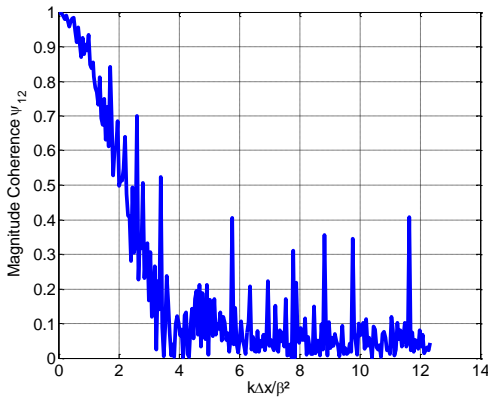616 distribution is plotted in figure 7c, where again good agreement is observed.

617

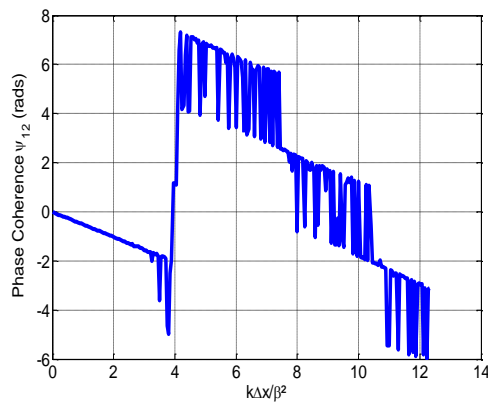Figure 7a. Coherence function magnitude for M = 0.5 and δ= 2.

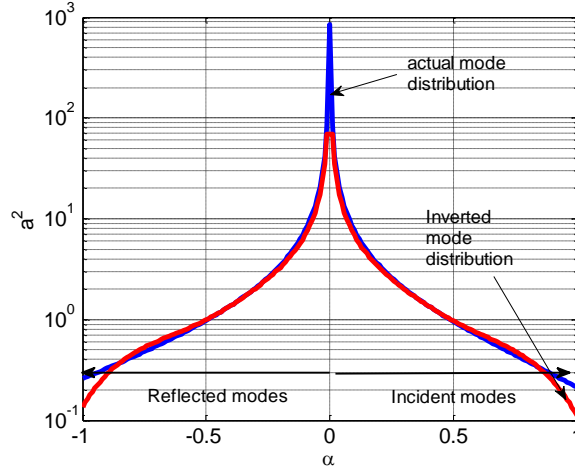Figure 7b. Predicted coherence (dashed curve) function phase for M = 0.5 and δ= 2.

618

619
620 Figure 7c. comparison of the exact (solid curves) and inverted mode amplitude distribution (dashed curves)
621 for four reflectivity factors.
622

623 **VI.   CONCLUSION AND DISCUSSION**

624 This paper has described a new method for determining the mode amplitude distribution versus modal cuton

625 ratio in multi-mode broadband sound field in ducts in the presence of uniform mean flow and reflections. The

626 novelty of the technique is that it requires only measurements of the complex coherence function made at the

627 duct wall. The measurement method makes the four important assumptions about the sound field:

628
629   1. The mode amplitude distribution is separable in the form, $E\left\{\left|A_{mn}^{\pm}(\omega)\right|^{2}\right\}=S(\omega)\overline{a_{\pm}^{2}}(\alpha_{mn})$

630   2. All propagating modes are mutually incoherent.
631
632   3. The number of modes that are able to propagate is sufficiently high that the mode distribution versus
633   α may be regarded as a continuous function and the modal sum replaced by an integration.
634
635   4. Mean flow is an axial 'plug 'flow'.
636

637
638   Assumption 1 is satisfied for any spatial distribution of sources[10,14], while assumption 2 is valid for

639 stochastic sources with length-scales much shorter than the acoustic wavelength. Examples of the latter are

640 fan broadband noise generated through the interaction between outlet guide vanes and rotor wake

641 turbulence, and the noise generated by unsteady combustion. Our experience has demonstrated that

642 Assumption 3 is sufficiently valid at non-dimensional frequencies of $ka > 10$, in which there are at least 30

643 propagating modes. In practical cases, this condition corresponds to a frequency of about 1.1 kHz for a duct

644   diameter of 1 m and above 22 kHz (beyond the audible range) for a duct diameter of 0.05 m. The method is

645   therefore appropriate to relatively large duct diameters, such as turbofan engines and large exhaust stacks.

646   Assumption 4 will never be strictly satisfied in flow ducts due to the presence of boundary layers at the duct

647   wall. In these cases, the relationship between the modal axial wavenumber and a in Eqs. (3) will be more

648   complicated and must be determined from the modal eigenvalues determined from numerical methods.

649   However, it is unlikely that axial flow speed variations of less than about 20% will significantly alter the

650   variation of mode amplitude with a, although more work is needed to confirm this assumption and extend the

651   measurement method to realistic flow profiles.

652

653   One practical difficulty with making the accurate coherence measurements of the acoustic field is the

654   presence of extraneous noise due to flow passing over the microphones. A well-known method to reduce the

655   effects of flow noise on duct wall measurements is to recess the microphones[15]. Subsonically convecting flow

656   disturbances will radiate to the recessed microphones as evanescent waves while acoustic noise will reach

657   the microphones un-attenuated.

658

References

[1] P. Joseph, "A Coherence Approach to Characterizing Broadband Sound Fields in Ducts," InterNoise 2014, 16th – 19th November, Melbourne, Australia.

[2] C. Moore, C., "Measurement of Radial and Circumferential Modes in Annular and Circular Ducts," Journal of Sound and Vibration, Vol. 62, No. 2, 1979, pp. 235-256.

[3] R. H. Thomas, F. Farassat, L. R. Clark, C. H. Gerhold, J. J. Kelly, and L. E. Becker. "A mode detection method using the azimuthal directivity of a turbofan model," AIAA paper 99-1954, 1999.

[4] F. Farassat, D. Nark, and H. Russel, "The detection of radiated modes from ducted fan engine," in *the Seventh AIAA/CEAS Aeroacoustics Conference*, Maastricht, The Netherlands, 2001, Paper No. AIAA 2001-2138.

[5] S. Lewy, "Inverse method predicting spinning modes radiated by a ducted fan from free-field measurements," J. Acoust. Soc. Am. **117**, 744–750 _2005_.

[6] U. Tapken, T. Raitor, L. "Enghardt. Tonal Noise Radiation from an UHBR Fan Optimized In-Duct Radial Mode Analysis." AIAA 2009-3288. 15th AIAA/CEAS Aeroacoustics, 11 - 13 May 2009, Miami, Florida.

[7] M. Abom, "Modal decomposition in ducts based on transfer function measurements between microphone pairs" Journal of Sound and Vibration **135**(1):95-114 (1989).

[8] C. R. Lowis, P. F. Joseph, A. J. Kempton, "Estimation of the far-field directivity of broadband aeroengine fan noise using an in-duct axial microphone array**."** Journal of Sound and Vibration, **329**, Issue 19, p. 3940-3957 (2010)

[9] E. J. Rice, "Multimodal far-field acoustic radiation pattern using mode cutoff ratio", AIAA Journal. **16**, 906–911 (1978)

[10] P. Joseph,, C.L. Morfey, C.R. Lowis, "Multi-mode sound transmission in ducts with flow", Journal of Sound and Vibration **264** 523–544 (2003).

[11] P. Joseph and C. L. Morfey, "Multi-mode radiation from an unflanged, semi-infinite circular duct", Journal of the acoustical society of America **105**(5), 2590 – 2600 (1999).

[12] S. Sinayoko, P. Joseph and A. McAlpine, "Multi-mode radiation from ducts with flow", Journal of the acoustical society of America. **127**(4) (2010).

[13] J. Melling, J. Chen, P. Joseph, "Experimental investigation of a new two-microphone method for the determination of broadband noise radiation from ducts"Applied Acoustics **117** (2017) 66–75.

[14] C.L. Morfey, "Sound transmission and generation in ducts with flow", Journal of Sound and Vibration **14**, 37 – 55 (1971).

[15] V. Fleury, L. Coste, R. Davy, A. Mignosi, C. Cariou, and J.-M. Prosper, "Optimization of Microphone Array Wall-Mountings in Closed-Section Wind Tunnels". AIAA 2010-3738, 16th AIAA/CEAS Aeroacoustics Conference (2010).